APRIL 01 2015

Exploring the resonant vibration of thin plates: Reconstruction of Chladni patterns and determination of resonant wave numbers

P. H. Tuan; C. P. Wen; P. Y. Chiang; ... et. al

J Acoust Soc Am 137, 2113–2123 (2015)
https://doi.org/10.1121/1.4916704

Exploring the resonant vibration of thin plates: Reconstruction of Chladni patterns and determination of resonant wave numbers

P. H. Tuan, C. P. Wen, P. Y. Chiang, and Y. T. Yu
Department of Electrophysics, National Chiao Tung University, 1001 Ta-Hsueh Road, Hsinchu 30010, Taiwan

H. C. Liang
Institute of Optoelectronic Science, National Taiwan Ocean University, 2 Pei-Ning Road, Keelung 20224, Taiwan

K. F. Huang and Y. F. Chen[a)]
Department of Electrophysics, National Chiao Tung University, 1001 Ta-Hsueh Road, Hsinchu 30010, Taiwan

(Received 30 September 2014; revised 10 March 2015; accepted 20 March 2015)

The Chladni nodal line patterns and resonant frequencies for a thin plate excited by an electronically controlled mechanical oscillator are experimentally measured. Experimental results reveal that the resonant frequencies can be fairly obtained by means of probing the variation of the effective impedance of the exciter with and without the thin plate. The influence of the extra mass from the central exciter is confirmed to be insignificant in measuring the resonant frequencies of the present system. In the theoretical aspect, the inhomogeneous Helmholtz equation is exploited to derive the response function as a function of the driving wave number for reconstructing experimental Chladni patterns. The resonant wave numbers are theoretically identified with the maximum coupling efficiency as well as the maximum entropy principle. Substituting the theoretical resonant wave numbers into the derived response function, all experimental Chladni patterns can be excellently reconstructed. More importantly, the dispersion relationship for the flexural wave of the vibrating plate can be determined with the experimental resonant frequencies and the theoretical resonant wave numbers. The determined dispersion relationship is confirmed to agree very well with the formula of the Kirchhoff–Love plate theory.
[http://dx.doi.org/10.1121/1.4916704]

[KML] Pages: 2113–2123

I. INTRODUCTION

Experimental resonant states in driven oscillation systems are of great importance in probing eigenstates of theoretical counterparts in various scientific fields including macroscopic as well as microscopic worlds.[1,2] The mathematical similarity for the wave equation enables us to acquire deep insights into the quantum world via exploring the paradigmatic systems of the classical world.[3–5] The vibrating plate which has been systematically studied and popularized by Chladni[6] is one of the most historical and classical two-dimensional (2D) wave systems. The Chladni experiment has acted as a precursor for various fields of research, such as seismology,[7] musical instruments,[8] quantum billiards,[9] and nano-mechanics.[10,11] Chladni nodal line patterns are formed by the sand particles that stop at the nodes of the resonant modes on a vibrating plate. Nowadays, the Chladni experiment is performed by using an electronically controlled mechanical oscillator to locally drive the plate with variable frequency. It is worthwhile to note that when the sizes of sand particles are less than 0.1 mm, the grains may migrate to the antinodes to form the so-called inverse Chladni patterns.[12] Although experiments on inverse Chladni patterns are a new area of research, Chladni nodal line patterns have been widely demonstrated in popular science.[13]

Rayleigh originally proposed to analyze the standard Chladni patterns by exploiting the Helmholtz equation instead of the bi-harmonic equation.[14,15] Although Rayleigh's approach greatly reduces the mathematical complexity, experimental Chladni patterns cannot be directly reconstructed with the eigenmodes of the Helmholtz equations.[16,17] The discrepancy between experimental resonant modes and theoretical eigenmodes mainly comes from the fact that the vibrating plate is an open system strongly coupled to the driving exciter. It has been experimentally observed[18–20] that the strong coupling between the oscillation system and the driving source may cause the resonant frequencies to be significantly different from the eigenfrequencies, i.e., the so-called resonant frequency shifts.[21–23] Due to the shifts of resonant frequencies, the resonant mode is generally formed by a superposition of numerous degenerate eigenmodes or nearly degenerate eigenmodes, i.e., the so-called mode-mixing effect.[24–27] So far the principle for determining resonant frequencies has not been disclosed. Consequently, experimental Chladni patterns generated by a continuous oscillating source have not been well explained and reconstructed theoretically.

In this work, the resonant vibration of the thin plate is experimentally and theoretically explored. In the experimental

a)Author to whom correspondence should be addressed. Electronic mail: yfchen@cc.nctu.edu.tw

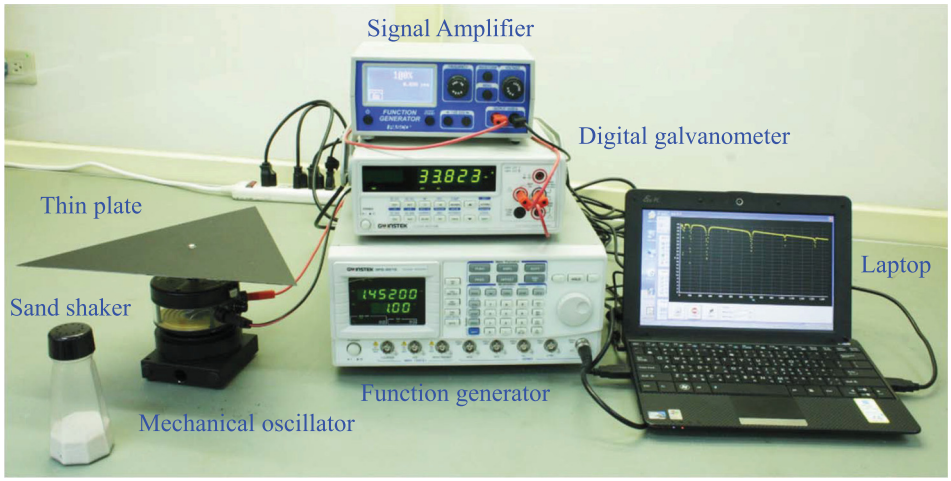

FIG. 1. (Color online) Experimental setup for measuring the spectrum of resonant frequencies and Chladni patterns.

aspect, an automatic scanning system is utilized to measure resonant frequencies and Chladni patterns of thin plates with square and equilateral triangle shapes. The resonant frequencies are fairly acquired with probing the variation of the effective impedance of the exciter with and without the thin plate. It is further experimentally confirmed that the Chladni resonant patterns are not affected by the ambient air and remain almost undisturbed as long as the extra masses are placed at the nodal lines or at the central excitation point. In the theoretical analysis, the inhomogeneous Helmholtz equation is exploited to derive the response function as a function of the driving wave number for exploring the vibrating wave on the thin plate. With the derived response function, the resonant wave numbers are theoretically identified with the maximum coupling efficiency as well as the maximum entropy principle.[28–31] Substituting the theoretical resonant wave numbers into the derived response function, it is numerically confirmed that the derived response function can be successfully used to reconstruct all experimental Chladni patterns. With the perfect reconstruction, the experimental resonant frequencies and the theoretical resonant wave numbers can be linked to obtain the dispersion relationships for the flexural wave of the vibrating plate. The determined dispersion relationship is confirmed to be in good agreement with the formula of the Kirchhoff–Love plate theory.

II. EXPERIMENTAL MEASUREMENT OF RESONANT CHLADNI PATTERNS

Figure 1 shows the experimental setup for measuring the spectrum of resonant frequencies and Chladni patterns. In experiment, we prepared a square plate with a side length of $a = 240$ mm and an equilateral triangle plate with a side length of $a = 289$ mm. Both thin plates were made of aluminum sheets with a thickness of $d = 1$ mm. The center of the thin plate was fixed with a screw supporter that was driven with an electronically controlled mechanical oscillator with sinusoidal wave of variable frequency.

For acquiring the resonant frequencies, we developed an auto-scanning system with 0.1-Hz resolution to measure the variation of the effective impedance of the mechanical oscillator without and with the thin plate.[32] When the mechanical oscillator was driven with an amplified sinusoidal voltage source, a digital galvanometer was connected in series with the mechanical oscillator to probe the effective current amplitude. As a consequence, the frequency response of the effective impedance of the mechanical oscillator could be accurately measured. Figure 2 shows experimental results for the frequency response of the effective impedance of the mechanical oscillator without (dashed line) and with (solid line) the thin plate. It can be seen that the frequency response of the effective impedance of the mechanical oscillator without the thin plate displays a monotonically increasing

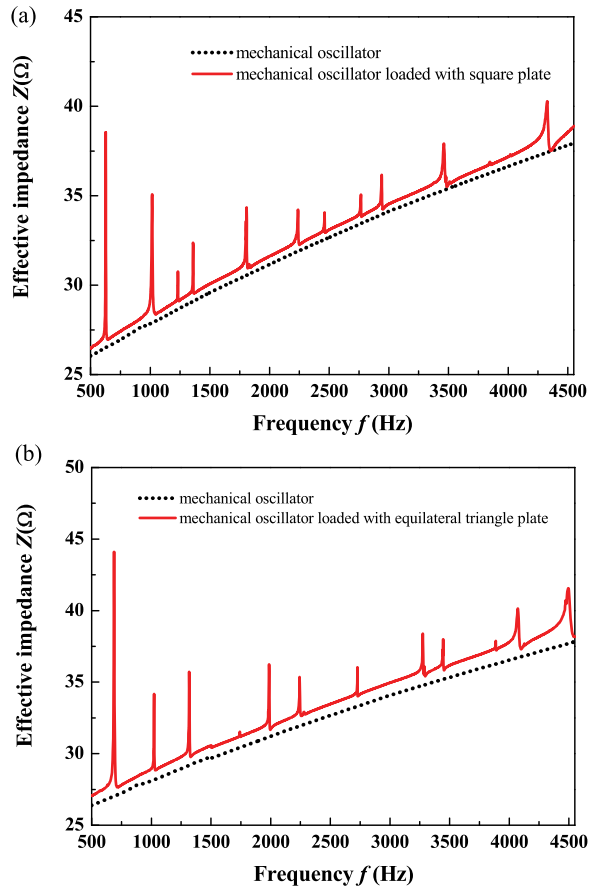

FIG. 2. (Color online) The measured effective impedances of the mechanical oscillator without (dashed line) and with (solid line) the (a) square and (b) equilateral triangle thin plates.

function, whereas there are numerous sharp peaks caused by the resonance to appear in the frequency spectrum with the thin plate. The resonant frequencies could be fairly acquired from the frequency response of the net impedance that was calculated by subtracting the effective impedance without the thin plate from that with the thin plate. Note that the influence of the extra mass effect from the central exciter on the measurement will be discussed later. Figures 3(a) and 4(a) show experimental results for the net impedances of the square and equilateral triangle vibrating plates, respectively. At each resonant frequency, 0.3-mm silica grains were used to manifest the so-called standard Chladni nodal line pattern. Figures 3(b) and 4(b) show experimental nodal line patterns captured with a camera at the resonant frequencies specified in Figs. 3(a) and 4(a), respectively. It is clear that all the Chladni patterns display the morphologies of wandering line structures that are conspicuously different from the regular nodal structures of eigenmodes.

To explore the influence of the ambient air on the resonant frequencies and Chladni patterns, the experiment of the vibrating plate, as shown in Fig. 5(a), was performed in a chamber with the air pressure reduced down to 10^{-1} Torr. It was found that the resonant frequency spectrum was nearly unchanged in comparison with the result obtained at the standard atmospheric pressure, as seen in Fig. 5(b). Besides, the resonant nodal line patterns were almost the same as those experimental results obtained at the standard atmospheric pressure.

Furthermore, the influence of the extra mass on measuring the resonant frequencies[33] and resonant nodal line patterns was also explored. At first, the mung beans which have significantly larger grain sizes and heavier masses in comparison with the silica sands were used as the granular media. Experimental results revealed that there are no noticeable differences between the resonant Chladni figures manifested by the mung beans and by the silica grains, as shown in Fig. 6(a). In this case, since the mung beans were finally located at the position of nodal lines where the vibrational amplitudes are very close to zero, the extra mass effect was minimal and the resonant frequencies were nearly unchanged. To examine the extra mass effect at the driving point where the vibrational amplitude is high, a concentrated mass M_{add} was deliberately added on the central screw supporter to remain the symmetry of the system. Figure 6(b) shows the resonant frequency spectra for the square plate measured under the cases with different M_{add}. Though some resonant peaks below 2000 Hz will shift to lower frequencies as M_{add} increases, it was confirmed that the small amount of drop in resonant frequencies will scarcely affect the resonant Chladni patterns. Since the mass of the screw supporter and the moving part of the exciter were estimated to be smaller than the used M_{add}, the extra mass effect from the central exciter on measuring the resonant frequencies and resonant Chladni patterns can be thus neglected in the present work. To be brief, the resonant frequencies measured by the proposed method were good approximations to the exact values.

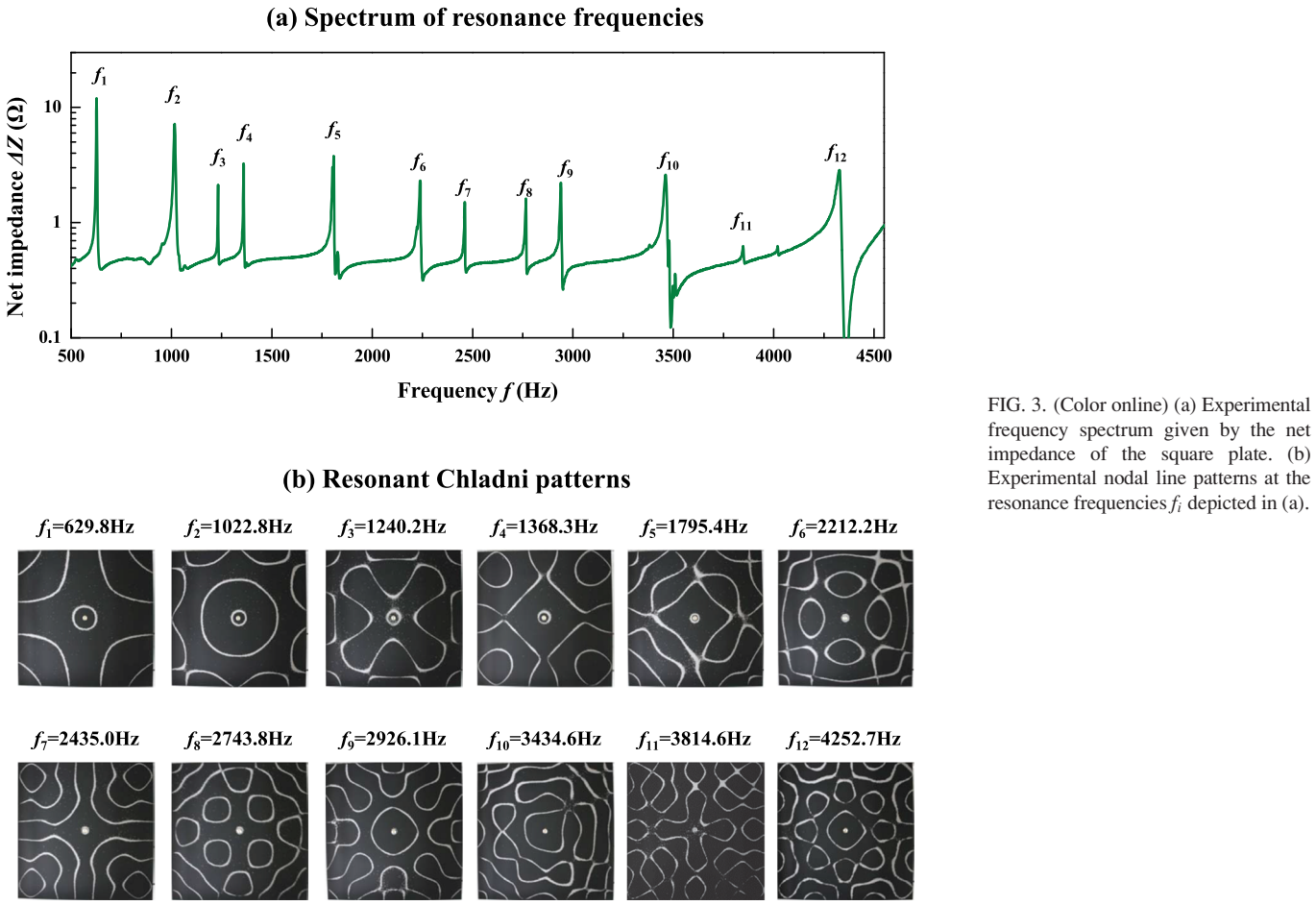

FIG. 3. (Color online) (a) Experimental frequency spectrum given by the net impedance of the square plate. (b) Experimental nodal line patterns at the resonance frequencies f_i depicted in (a).

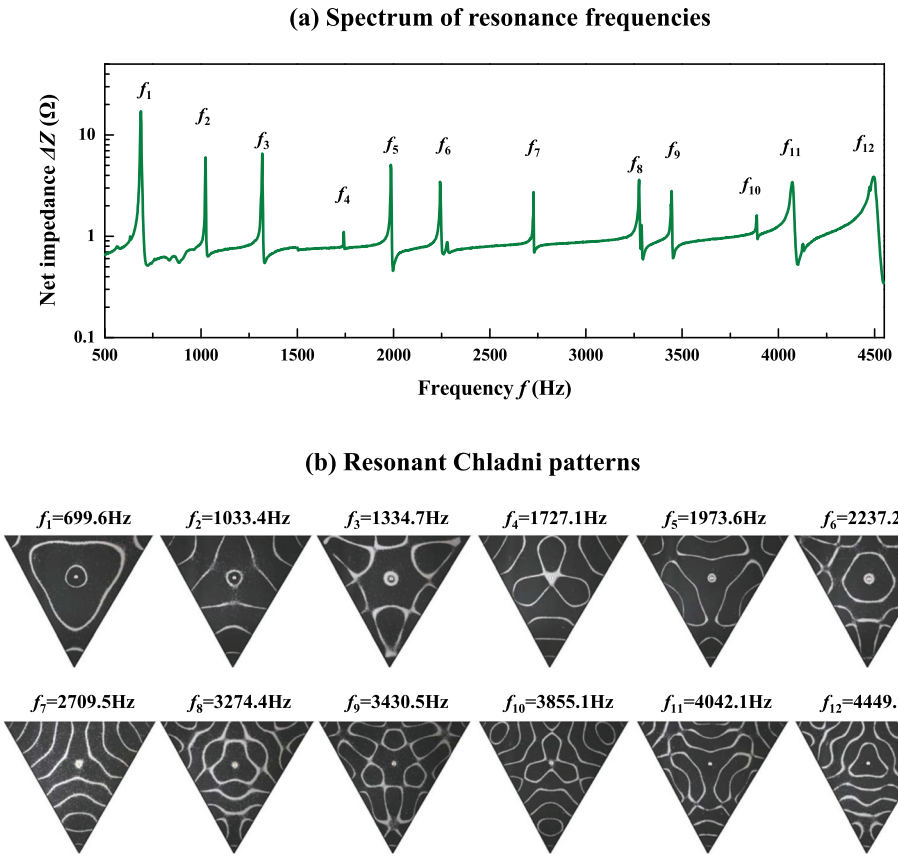

FIG. 4. (Color online) (a) Experimental frequency spectrum given by the net impedance of the equilateral triangle plate. (b) Experimental nodal line patterns at the resonance frequencies f_i depicted in (a).

III. THEORETICAL MODEL FOR RESONANT WAVE NUMBERS AND CHLADNI PATTERNS

Since Chladni's experiment is a driven oscillation system, we use the 2D inhomogeneous Helmholtz equation with the approach of Green's function to derive the response function of the thin plate. Note that the aspect ratio of the thickness to the lateral dimension for the studied plate is generally less than 0.02. As a result, the vibrating eigenmodes can be approximated with the 2D Helmholtz equation.[34] Considering a thin plate driven by a time-harmonic source $F(\mathbf{r}')$, the response function $\Psi(\mathbf{r};\ \mathbf{r}', \tilde{k})$ of the vibrating plate can be solved with the inhomogeneous Helmholtz equation

$$(\nabla^2 + \tilde{k}^2)\Psi(\mathbf{r};\ \mathbf{r}', \tilde{k}) = F(\mathbf{r}'), \tag{1}$$

where $\tilde{k} = k + i\gamma$, k is the driving wave number, and γ is the damping coefficient of the vibrating system. From the Kirchhoff–Love plate theory, the dispersion relation between the driving frequency and the driving wave number for the flexural wave is given by[13]

$$f(k) = C \cdot k^2 \tag{2}$$

with

$$C = \frac{1}{2\pi}\sqrt{\frac{Ed^2}{12\rho(1-\nu^2)}}, \tag{3}$$

where E is the Young's modulus, ν is the Poisson ratio, ρ is the mass density, and d is the thickness of plate. Since there are some uncertainties for the Young's modulus and the Poisson ratio, the precise value for the coefficient C in Eq. (3) is usually difficult to evaluate for real materials. Therefore, one of the most important aims in this work is to determine the coefficient C from the experimental resonant frequencies and the theoretical resonant wave numbers.

Due to the free edge of the vibrating plate, the vibrating wave function at the boundary $\partial\Omega$ must satisfy the Neumann-type boundary condition of $\partial\Psi/\partial n|_{\partial\Omega} = 0$ at the boundary $\partial\Omega$ of the thin plate. When the driving source is an ideal point source at $\mathbf{r} = \mathbf{r}'$, the response function in Eq. (1) is the so-called Green's function $G(\mathbf{r};\ \mathbf{r}', \tilde{k})$. In terms of the Green's function, the response function excited by any general source $F(\mathbf{r}')$ can be given by

$$\Psi(\mathbf{r};\ \mathbf{r}', \tilde{k}) = \int_V G(\mathbf{r};\ \mathbf{r}', \tilde{k})F(\mathbf{r}')d^3r'. \tag{4}$$

For the system with $\gamma \ll k$, the Green's function can be expanded with the eigenmodes as

$$G(\mathbf{r};\ \mathbf{r}', \tilde{k}) = \sum_n \frac{\Phi_n^*(\mathbf{r}') \cdot \Phi_n(\mathbf{r})}{(k^2 - k_n^2) + 2i\gamma k}, \tag{5}$$

where $\Phi_n(\mathbf{r})$ and k_n are the eigenmodes and eigenvalues, respectively. Substituting Eq. (5) into Eq. (4), the normalized response function $\Psi(\mathbf{r};\ \mathbf{r}', \tilde{k})$ is then given by

$$\Psi(\mathbf{r};\ \mathbf{r}', \tilde{k}) = \sum_n a_n(\mathbf{r}', \tilde{k})\,\Phi_n(\mathbf{r}), \tag{6}$$

(a)

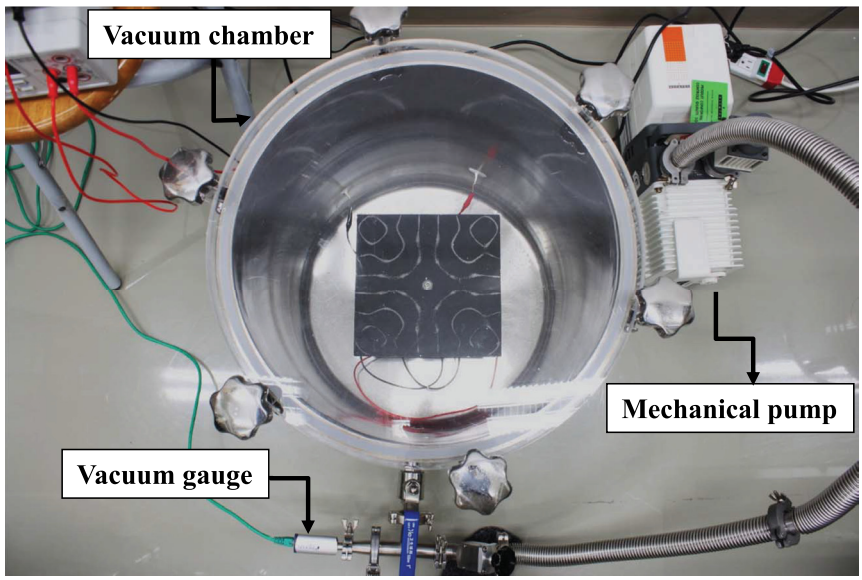

(b)

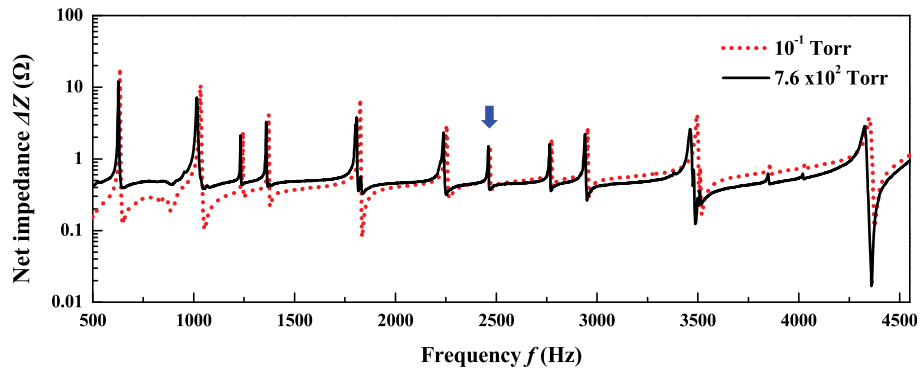

FIG. 5. (Color online) (a) The experimental system for exploring the influence of the ambient air on the resonant frequencies and Chladni patterns. The nodal line pattern shown in the photo is measured at the resonance frequency marked by the arrow in (b). (b) The net impedances of the square plate measured under different air pressures.

(a)

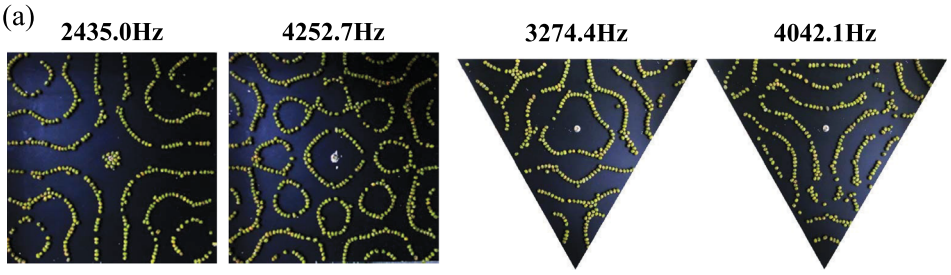

(b)

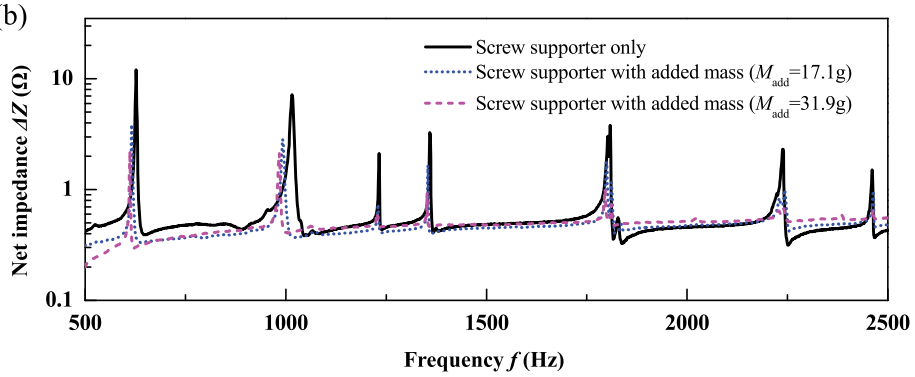

FIG. 6. (Color online) (a) Some resonant Chladni figures manifested by the mung beans as the granular media. (b) The resonant frequencies spectra measured under the cases with different added mass M_{add} at the central driving point.

with the coefficient

$$a_n(\mathbf{r}', \tilde{k}) = \frac{A_n(\mathbf{r}', \tilde{k})}{\sqrt{\sum_n |A_n(\mathbf{r}', \tilde{k})|^2}}, \tag{7}$$

$$A_n(\mathbf{r}', \tilde{k}) = \frac{\int \Phi_n^*(\mathbf{r}') F(\mathbf{r}')\, d^3 r'}{(k^2 - k_n^2) + 2\, i\, \gamma\, k}. \tag{8}$$

The denominator in the right-hand side of Eq. (8) indicates that the vibrating wave function is mainly formed by the eigenmodes $\Phi_n(\mathbf{r})$ with eigenvalues k_n close to the driving wavenumber k. It is worthwhile to mention that the mathematical form in the denominator of Eq. (8) is similar to the Breit-Wigner formula for expressing the resonant states in quantum systems.[35] The numerator in the right-hand side of Eq. (8) also reveals that the overlap integral between the eigenmode $\Phi_n(\mathbf{r}')$ and the source $F(\mathbf{r}')$ plays an important role in the vibrating wave function.

Since there was no theoretical model to determine the resonant wave numbers in past investigations, the reconstruction for Chladni figures was unsolved so far. To explore a fundamental principle for determining the resonant wave numbers in the Chladni experiment, we consider the coupling efficiency of the power transfer from the external source to the plate system. According to theoretical acoustics,[36] the power transferred from the driving source to the mechanical vibrating system is proportional to the absolute square of the time-derivative of the response mode, i.e., $\eta \propto |\partial \Psi / \partial t|^2$. Under a time-harmonic condition, the effective coupling efficiency of the normalized power transferred from the point source to the vibrating plate can be given by

$$\eta(\mathbf{r}', \tilde{k}) = \left| \sum_n {k_n}^2 \cdot a_n(\mathbf{r}\prime, \tilde{k}) \cdot \Phi_n(\mathbf{r}\prime) \right|^2. \tag{9}$$

Here we have used the quadratic dispersion relation of the plate and omit the common constants that will not affect the relative results. From another point of view, the coupling strength between the thin plate and the driving source can be evaluated with the number of effective participated eigenmodes.[37,38] Entropy is a logarithmic measure of the number of eigenmodes with significant participated probability. The information entropy of the response function in Eq. (6) can be calculated as a function of the driving wave number. From the Shannon theory[29] and in term of the coefficient in Eq. (7), the information entropy of the response function $\Psi(\mathbf{r};\ \mathbf{r}', \tilde{k})$ is given by

$$S(\mathbf{r}', \tilde{k}) = -\sum_n p_n(\mathbf{r}', \tilde{k}) \ln[p_n(\mathbf{r}', \tilde{k})], \tag{10}$$

where $p_n(\mathbf{r}', \tilde{k}) = |a_n(\mathbf{r}', \tilde{k})|^2$ represents the probability of the eigenmode $\Phi_n(\mathbf{r})$ in the response function $\Psi(\mathbf{r};\ \mathbf{r}', \tilde{k})$. Considering a mixed state that is superposed by N eigenmodes with equal probabilities, i.e., $p_n = 1/N$, the formula in Eq. (10) can be used to obtain $S = \ln N$. Therefore, the exponential form of $\exp[S(\mathbf{r}', \tilde{k})]$ can be practically used to evaluate the effective number of participated eigenmodes N_{eff} in the response function. In Sec. IV, it is verified that the maximum entropy principle can be exploited to obtain the resonant wave numbers in a direct way.

IV. NUMERICAL VERIFICATION AND DETERMINATION OF DISPERSION RELATIONS

Now considering a square-shape plate with the region in $0 \le x, y \le a$, the eigenmodes are given by

$$\Phi_{n_1,n_2}(x, y) = \frac{2}{a} \cos\left(\frac{n_1 \pi}{a} x\right) \cos\left(\frac{n_2 \pi}{a} y\right), \tag{11}$$

where $n_1 = 0, 1, 2, 3, \ldots$ and $n_2 = 0, 1, 2, 3, \ldots$. The eigenvalues corresponding to the eigenmodes $\Phi_{n_1,n_2}(x, y)$ are given by

$$k_{n_1,n_2} = \frac{\pi}{a} \sqrt{n_1^2 + n_2^2}. \tag{12}$$

With a point source at the center, the driving function can be expressed as

$$F(\mathbf{r}') = F_o\, \delta(x' - a/2) \delta(y' - a/2), \tag{13}$$

where F_o is the amplitude of the driving source. Substituting Eqs. (11)–(13) into Eq. (6), the normalized wave function is given by

$$\Psi(x, y;\ \tilde{k}) = \sum_{n_1,n_2} a_{n_1,n_2}(\tilde{k})\, \Phi_{n_1,n_2}(x, y), \tag{14}$$

with the coefficient

$$a_{n_1,n_2}(\tilde{k}) = \frac{A_{n_1,n_2}(\tilde{k})}{\sqrt{\sum_{n_1,n_2} |A_{n_1,n_2}(\tilde{k})|^2}}, \tag{15}$$

$$A_{n_1,n_2}(\tilde{k}) = F_o \frac{\Phi_{n_1,n_2}(a/2, a/2)}{(k^2 - k_{n_1,n_2}^2) + 2\, i\, \gamma\, k}. \tag{16}$$

Note that since the point source is located at the center of the square, the numerator in the right-hand side of Eq. (15) allows only eigenmodes with both even indices of n_1, n_2 in the superposition. With Eqs. (14)–(16), the wave patterns $|\Psi(x, y;\ \tilde{k})|^2$ can be calculated by inputting different values of the driving wave number and a fixed damping factor. From the width of the resonance peaks, the value of the damping factor γ was found to be approximately $0.02\ a^{-1}$. Note that the value of the amplitude of the driving source F_o will not affect the morphology of a wave pattern in the calculation. Substituting Eqs. (15) and (16) into Eq. (10) and with $\gamma = 0.02\ a^{-1}$, the information entropy for the square plate with the central driving can be numerically computed as a function of the driving wave number. On the other hand, substituting Eqs. (15) and (16) into Eq. (9), the power transferred efficiency $\eta(\mathbf{r}', \tilde{k})$ for the square plate can be numerically calculated as a function of the driving wave number. Figures 7(a) and 7(b) show the calculated results versus the driving wave number for the entropy distribution

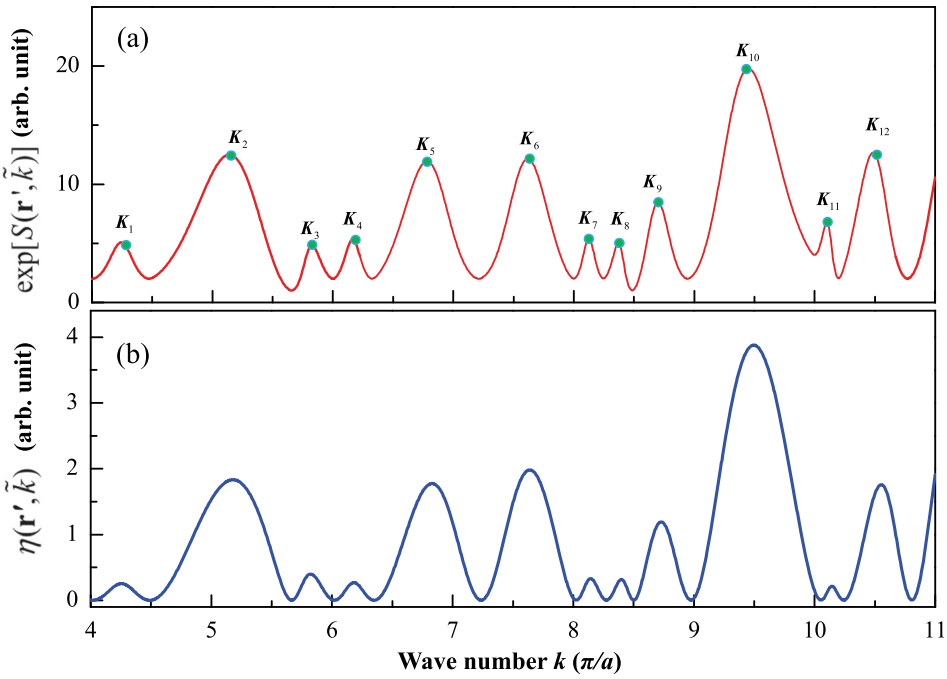

FIG. 7. (Color online) Calculated results of the (a) entropy distribution $e^{S(\mathbf{r}',\tilde{k})}$ and (b) power transferred efficiency $\eta(\mathbf{r}',\tilde{k})$ as a function of the driving wave number for the square plate.

$\exp[S(\mathbf{r}',\tilde{k})]$ and power transferred efficiency $\eta(\mathbf{r}',\tilde{k})$, respectively. It can be seen that the peak positions of $\eta(\mathbf{r}',\tilde{k})$ are utterly consistent with those of entropy distribution $\exp[S(\mathbf{r}',\tilde{k})]$. The driving wave numbers k corresponding to the peak positions are the theoretical resonant wave numbers and are denoted as K_n with $n = 1, 2, 3, ...$, as shown in Fig. 7(a).

Substituting $\tilde{k} = K_n + i\gamma$ into Eqs. (14)–(16), the wave patterns $|\Psi(x, y; \tilde{k})|^2$ corresponding to the resonant modes can be calculated to make a comparison with experimental Chladni patterns shown in Fig. 3(b). Figure 8(a) shows the numerical nodal line patterns calculated with $\tilde{k} = K_n + i\gamma$ and Eqs. (14)–(16). Note that the theoretical nodal line patterns are plotted by the inverse of the wave patterns $|\Psi(x, y; \tilde{k})|^2$ for manifestation. It is clear that the theoretical nodal line patterns are in good agreement with the experimental Chladni patterns shown in Fig. 3(b) for all cases. The perfect agreement indicates that the spectrum of resonant wave numbers can be accurately determined by the driving wave numbers to lead to the local maxima in the entropy distribution $\exp[S(\mathbf{r}',\tilde{k})]$. To be brief, experimental Chladni patterns can be theoretically reconstructed by using the response function $\Psi(\mathbf{r}; \mathbf{r}',\tilde{k})$ in Eq. (6) with the driving wave numbers at the local maxima of the entropy distribution $\exp[S(\mathbf{r}',\tilde{k})]$ from Eq. (10). Figure 8(b) shows a comparison between the theoretical resonant wave numbers K_n and

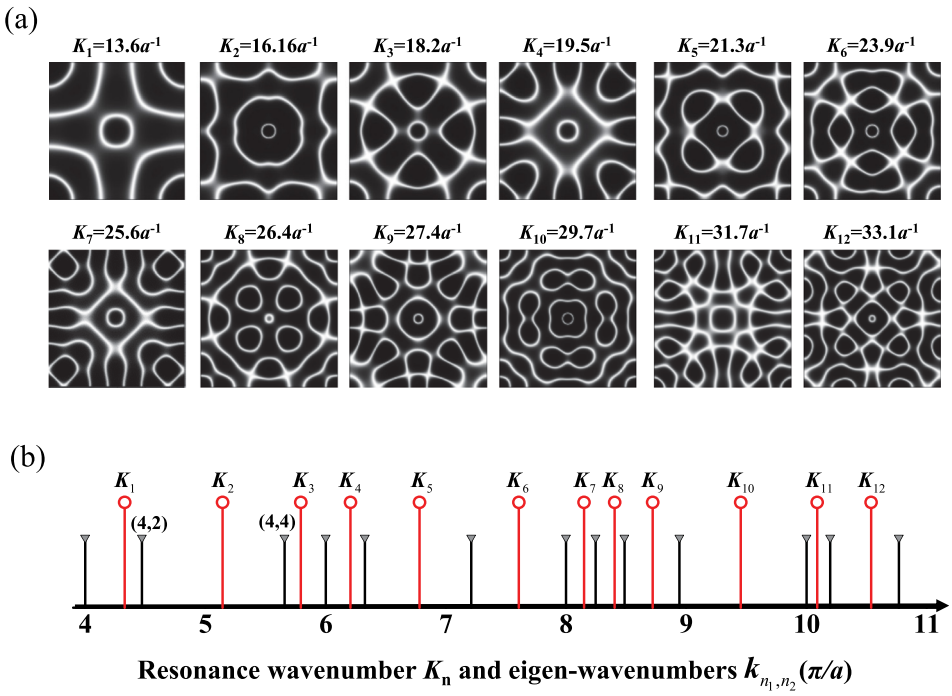

FIG. 8. (Color online) (a) Numerically reconstructed nodal line patterns corresponding to the experimental Chladni figures shown in Fig. 3(b). (b) A comparison between the resonant wave numbers K_n and the eigenvalues k_{n_1,n_2}.

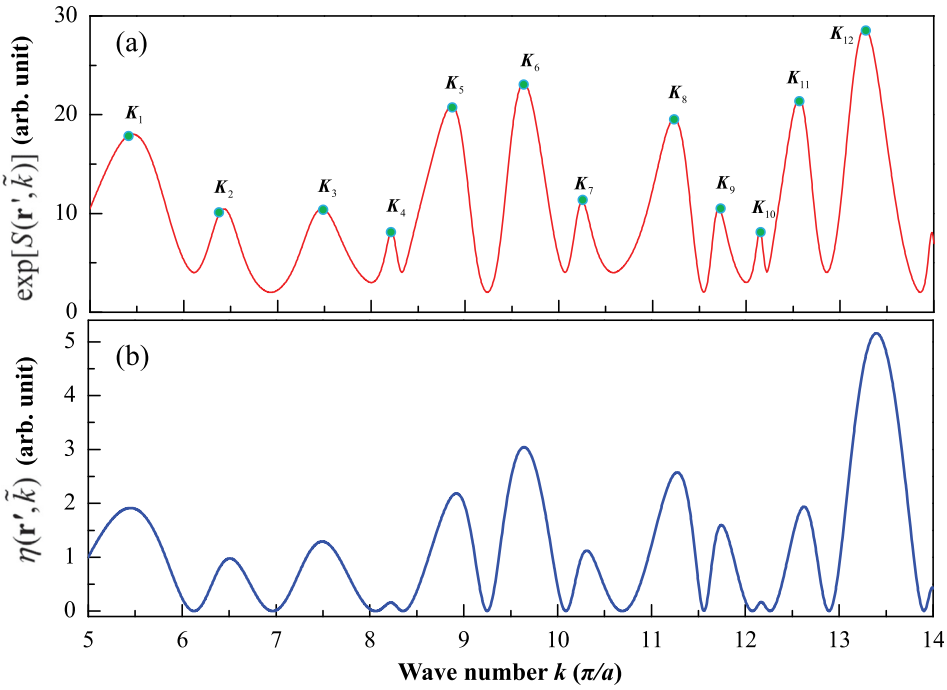

FIG. 9. (Color online) Calculated results of the (a) entropy distribution $e^{S(\mathbf{r}',\tilde{k})}$ and (b) power transferred efficiency $\eta(\mathbf{r}',\tilde{k})$ as a function of the driving wave number for the equilateral triangle plate.

the eigenvalues k_{n_1,n_2}. The K_n spectrum is conspicuously different from the distribution of eigenvalues k_{n_1,n_2}. This result indicates that the effect of resonant frequency shifts[21–23] is extremely significant in the resonant vibration of thin plates for the Chladni experiment under the continuous excitation.

The same procedure was employed to analyze experimental results obtained with the equilateral triangle thin plate. The eigenmodes of an equilateral triangle vibrating plate can be categorized into two types of degenerate modes with odd and even symmetries.[39] Considering the plate with vertices at $(0, 0)$, $(a/2, \sqrt{3}a/2)$, and $(-a/2, \sqrt{3}a/2)$, the eigenmodes can be expressed as

$$\begin{Bmatrix} \Phi^{(o)}_{n_1,n_2}(x,y) \\ \Phi^{(e)}_{n_1,n_2}(x,y) \end{Bmatrix} = \sqrt{\frac{16}{a^2 3\sqrt{3}}} \left\{ \begin{matrix} \sin \\ \cos \end{matrix} \left[\frac{2\pi}{3a}(2n_1 - n_2)x\right] \cos\left(\frac{2\pi}{\sqrt{3}a} n_2 y\right) + \begin{matrix} \sin \\ \cos \end{matrix} \left[\frac{2\pi}{3a}(2n_2 - n_1)x\right] \cos\left(\frac{2\pi}{\sqrt{3}a} n_1 y\right) + \begin{matrix} \sin \\ \cos \end{matrix} \left[-\frac{2\pi}{3a}(n_1 + n_2)x\right] \cos\left[\frac{2\pi}{\sqrt{3}a}(n_1 - n_2)y\right] \right\}, \tag{17}$$

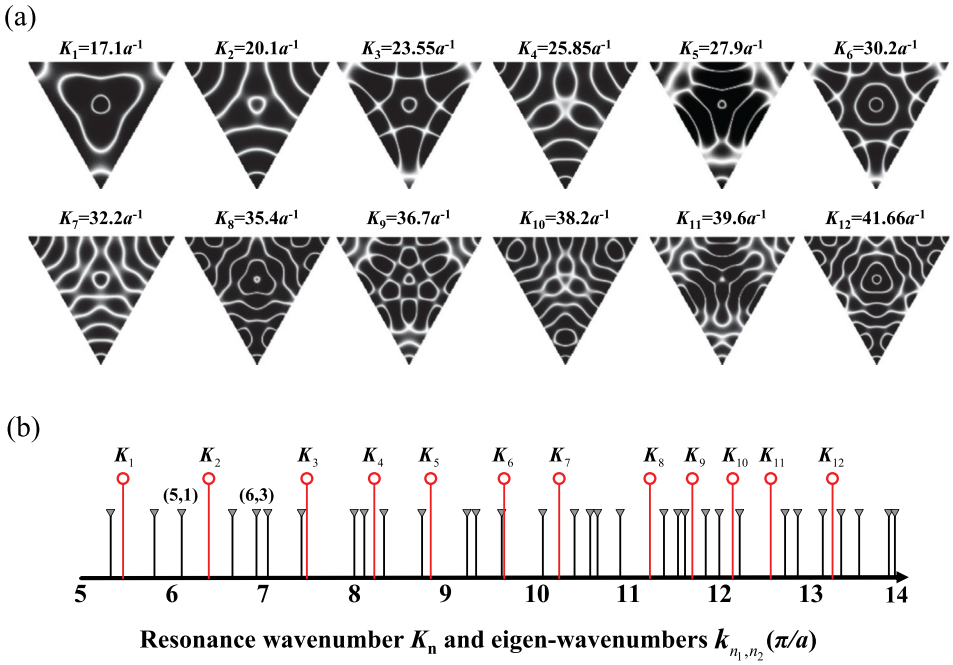

FIG. 10. (Color online) (a) Numerically reconstructed nodal line patterns corresponding to the experimental Chladni figures shown in Fig. 4(b). (b) A comparison between the resonant wave numbers K_n and the eigenvalues k_{n_1,n_2}.

where $n_1 = 0, 1, 2, 3, \ldots$, $n_2 = 0, 1, 2, 3, \ldots$, and the odd and even symmetries are denoted by the superscripts (o) and (e), respectively. The eigenvalues for the eigenmodes $\Phi^{(o)}_{n_1,n_2}(x,y)$ and $\Phi^{(e)}_{n_1,n_2}(x,y)$ are given by

$$k_{n_1,n_2} = \frac{4\pi}{3a}\sqrt{n_1^2 + n_2^2 - n_1 n_2}. \tag{18}$$

With a point source at the center of the thin plate, the source function can be expressed as

$$F(\mathbf{r}') = F_o\,\delta(x')\delta(y' - a/\sqrt{3}), \tag{19}$$

where F_o is the amplitude of the driving source. Substituting Eqs. (17)–(19) into Eq. (6), the normalized response function of the thin plate is given by

$$\Psi(x,y;\tilde{k}) = \sum_{n_1,n_2} a_{n_1,n_2}(\tilde{k})\,\Phi^{(e)}_{n_1,n_2}(x,y), \tag{20}$$

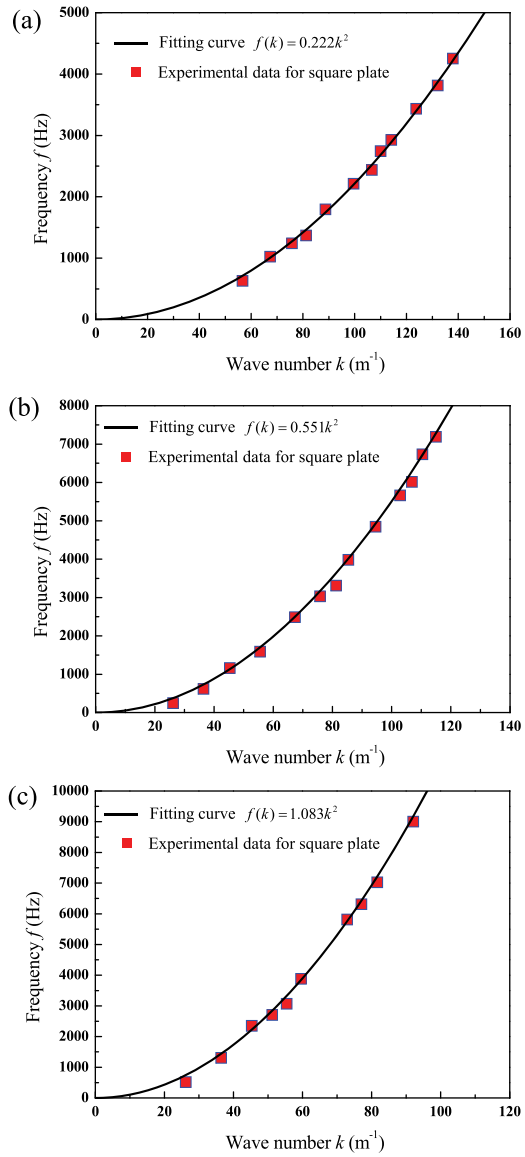

FIG. 11. (Color online) The dispersion curves determined by the experimental resonant frequencies and theoretical resonant wave numbers of the square aluminum plates with the thickness d of (a) 1 mm, (b) 2 mm, and (c) 5 mm.

with the coefficient

$$a_{n_1,n_2}(\tilde{k}) = \frac{A_{n_1,n_2}(\tilde{k})}{\sqrt{\sum_{n_1,n_2}|A_{n_1,n_2}(\tilde{k})|^2}}, \tag{21}$$

$$A_{n_1,n_2}(\tilde{k}) = F_o\,\frac{\Phi^{(e)}_{n_1,n_2}(0, a/\sqrt{3})}{(k^2 - k^2_{n_1,n_2}) + 2i\gamma k}. \tag{22}$$

Note that only eigenmodes with even symmetry have contributions in the response function of Eqs. (20) and (22) due to the symmetry of the source function in Eq. (19).

Substituting Eqs. (21) and (22) into Eqs. (9) and (10) and using $\gamma = 0.02a^{-1}$, the power transferred efficiency $\eta(\mathbf{r}', \tilde{k})$ and the entropy distribution $\exp[S(\mathbf{r}', \tilde{k})]$ for the equilateral triangle plate can be calculated with the driving wave number as a variable. Figures 9(a) and 9(b) show the calculated results versus the driving wave number for the entropy distribution $\exp[S(\mathbf{r}', \tilde{k})]$ and power transferred efficiency $\eta(\mathbf{r}', \tilde{k})$, respectively. Again, the variation of the power transferred efficiency $\eta(\mathbf{r}', \tilde{k})$ completely resembles that of the entropy distribution $\exp[S(\mathbf{r}', \tilde{k})]$. The theoretical resonant wave numbers K_n with $n = 1, 2, 3, \ldots$ are similarly identified with the peak positions, as shown in Fig. 9(a).

Figure 10(a) shows the numerical nodal line patterns calculated with $\tilde{k} = K_n + i\gamma$ and Eqs. (20)–(22) to make a comparison with experimental Chladni patterns shown in Fig. 4(b). Once again, it is clear that the theoretical nodal line patterns agree very well with the experimental Chladni patterns shown in Fig. 4(b) for all cases. Figure 10(b) shows a comparison between the theoretical resonant wave numbers K_n and the eigenvalues k_{n_1,n_2}. As expected, the spectrum of resonant wave numbers K_n is considerably different from the distribution of eigenvalues k_{n_1,n_2}.

Finally, it is useful to discuss that the dispersion relationship for the flexural wave of the vibrating plate can be precisely determined with the experimental resonant frequencies and the theoretical resonant wave numbers. Figure 11(a) shows the dispersion curve determined by the experimental resonant frequencies and the theoretical resonant wave numbers for the square plate with $d = 1$ mm. With the

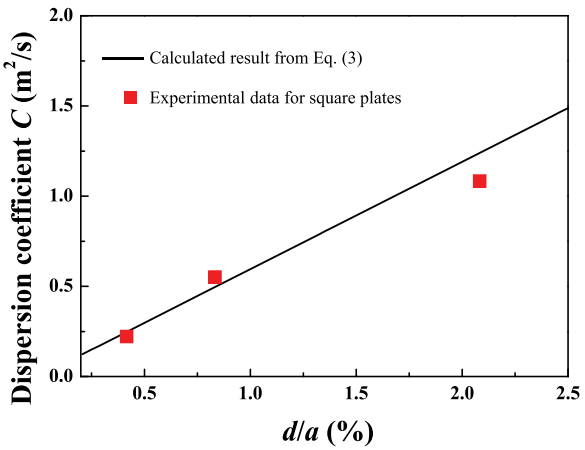

FIG. 12. (Color online) Comparison between the fitting coefficient C and the theoretical formula in Eq. (3) for the plates with different ratios of d/a.

formula in Eq. (2) for the best fitting to the determined results, the coefficient C is found to be approximately 0.222. It is intriguing that the value of $C = 0.222$ is quite close to the theoretical value of 0.246 calculated by Eq. (3) with the material parameters for the aluminum plate: $E = 69\,\text{GPa}$, $\nu = 0.33$, $\rho = 2700\,\text{kg/m}^3$, and $d = 1\,\text{mm}$. With the same approach, the dispersion relationship for the square plates with $d = 2\,\text{mm}$ and $d = 5\,\text{mm}$ are also determined, as shown in Figs. 11(b) and 11(c). The values of the best fitting coefficient C are approximately 0.551 and 1.083 for $d = 2\,\text{mm}$ and $d = 5\,\text{mm}$, respectively. Figure 12 shows a comparison between the fitting coefficient C and the theoretical formula in Eq. (3) for the plate with different ratios of d/a. It can be seen that the trend of the determined coefficient C agrees very well with the theoretical calculation. The good agreement further confirms the validity of the present theoretical model for analyzing the flexural wave in the vibrating thin plate and determining the dispersion relationship.

V. CONCLUSIONS

The Chladni nodal line patterns and resonant frequencies for a thin plate excited by an electronically controlled mechanical oscillator have been experimentally measured. The resonant frequencies were fairly attained by means of probing the difference between the effective impedances of the exciter with and without the thin plate. Furthermore, it has been experimentally confirmed that the Chladni resonant patterns are almost not affected by the ambient air and remain almost undisturbed as long as the extra masses are placed at the nodal lines or at the central excitation point. In the theoretical aspect, the inhomogeneous Helmholtz equation has been employed to derive the response function for the vibrating wave on the thin plate as a function of the driving wave number. From the viewpoint of the maximum coupling efficiency as well as the maximum entropy principle, the derived response function is directly used to theoretically identify the resonant wave numbers. It has been evidenced that the derived response function with the theoretically resonant wave numbers can excellently reconstruct all experimental Chladni patterns. The experimental resonant frequencies and the theoretical resonant wave numbers were further combined to deduce the dispersion relationships for the flexural wave of the vibrating plate. Finally, the determined dispersion relationship has been confirmed to be nicely consistent with the formula of the Kirchhoff–Love plate theory.

ACKNOWLEDGMENTS

The authors acknowledge the Ministry of Science and Technology in Taiwan for their financial support of this research under Contract No. MOST-103-212-M-009-016-MY3.

[1]M. Brack and R. K. Bhaduri, *Semiclassical Physics* (Addison-Wesley, Reading, MA, 1997), pp. 1–437.
[2]M. C. Gutzwiller, *Chaos in Classical and Quantum Mechanics* (Springer, New York, 1990), pp. 1–427.
[3]P. A. Chinnery and V. F. Humphrey, "Experimental visualization of acoustic resonances within a stadium-shaped cavity," Phys. Rev. E **53**, 272–276 (1996).
[4]K. Schaadt, T. Guhr, C. Ellegaard, and M. Oxborrow, "Experiments on elastomechanical wave functions in chaotic plates and their statistical features," Phys. Rev. E **68**, 036205 (2003).
[5]J. Stein and H.-J. Stöckmann, "Experimental determination of billiard wave functions," Phys. Rev. Lett. **68**, 2867–2870 (1992).
[6]Lord Rayleigh, "On the calculation of Chladni's figures for a square plate," Philos. Mag. **22**, 225–229 (1911).
[7]J. Flores, "Nodal patterns in the seismic response of sedimentary valleys," Eur. Phys. J. Special Topics **145**, 63–75 (2007).
[8]N. E. Molin, L.-E. Lindgren, and E. V. Jansson, "Parameters of violin plates and their influence on the plate modes," J. Acoust. Soc. Am. **83**, 281–291 (1988).
[9]K. Schaadt and A. Kudrolli, "Experimental investigation of universal parametric correlators using a vibrating plate," Phys. Rev. E **60**, R3479–R3482 (1999).
[10]M. Dorrestijn, A. Bietsch, T. Açıkalın, A. Raman, M. Hegner, E. Meyer, and Ch. Gerber, "Chladni figures revisited based on nanomechanics," Phys. Rev. Lett. **98**, 026102 (2007).
[11]S. Chakram, Y. S. Patil, L. Chang, and M. Vengalattore, "Dissipation in ultrahigh quality factor SiN membrane resonators," Phys. Rev. Lett. **112**, 127201 (2014).
[12]H. Gerner, M. Hoef, D. Meer, and K. Weele, "Inversion of Chladni patterns by tuning the vibrational acceleration," Phys. Rev. E **82**, 012301 (2010).
[13]A. W. Leissa, *Vibration of Plates* (Acoustical Society of America, Woodbury, NY, 1993), pp. 1–345.
[14]T. Wah, "Vibration of circular plates," J. Acoust. Soc. Am. **34**, 275–281 (1962).
[15]Lord Rayleigh, *Theory of Sound* (Dover, New York, 1945), pp. 363–381.
[16]M. D. Waller, "Vibration of free circular plates. Part 2: Compounded normal modes," Proc. Phys. Soc. **50**, 77–82 (1938).
[17]M. D. Waller, "Vibration of free square plates: Part II: Compounded normal modes," Proc. Phys. Soc. **52**, 452–455 (1940).
[18]U. Kuhl, E. Persson, M. Barth, and H.-J. Stöckmann, "Mixing of wavefunctions in rectangular microwave billiards," Eur. Phys. J. B **17**, 253–259 (2000).
[19]I. V. Zozoulenko and K.-F. Berggren, "Quantum scattering, resonant states, and conductance fluctuations in an open square electron billiard," Phys. Rev. B **56**, 6931–6941 (1997).
[20]K. Schaadt, A. P. B. Tufaile, and C. Ellegaard, "Chaotic sound waves in a regular billiard," Phys. Rev. E **67**, 026213 (2003).
[21]A. Prak, F. R. Blom, M. Elwenspoek, and T. S. J. Lammerink, "Q-factor and frequency shift of resonating silicon diaphragms in air," Sens. Actuators A **27**, 691–698 (1991).
[22]M. Ikeda, M. Ignatenko, A. Mase, and K. Uchino, "Modeling and experimental detection of resonance frequency shift of a microwave cavity caused by a small conductive particle," J. Electromagn. Waves Appl. **27**, 1114–1126 (2013).
[23]J. Stein, H.-J. Stöckmann, and U. Stoffregen, "Microwave studies of billiard green functions and propagators," Phys. Rev. Lett. **75**, 53–56 (1995).
[24]G. B. Akguc and L. E. Reichl, "Conductance and statistical properties of chaotic and integrable electron waveguides," J. Stat. Phys. **98**, 813–834 (2000).
[25]A. F. Sadreev, "Current statistics for transport through rectangular and circular billiards," Phys. Rev. E **70**, 016208 (2004).
[26]K. Schaadt, G. Simon, and C. Ellegaard, "Ultrasound resonances in a rectangular plate described by random matrices," Phys. Scr. T **90**, 231–237 (2001).
[27]P. H. Tuan, C. P. Wen, Y. T. Yu, H. C. Liang, K. F. Huang, and Y. F. Chen, "Exploring the distinction between experimental resonant modes and theoretical eigenmodes: From vibrating plates to laser cavities," Phys. Rev. E **89**, 022911 (2014).
[28]P. Dey, D. Sarkar, A. Khan, and S. Basu, "Participation ratio and fidelity analyses as tools to study BCS-BEC crossover," Eur. Phys. J. B. **81**, 95–102 (2011).
[29]C. E. Shannon, "Prediction and entropy of printed English," Bell Syst. Tech. J. **30**, 50–64 (1951).
[30]E. T. Jaynes, "Information theory and statistical mechanics," Phys. Rev. **106**, 620–630 (1957).

[31]H. Haken, *Information and Self-Organization: A Macroscopic Approach to Complex Systems* (Springer-Verlag, Berlin, 2006), pp. 53–79.
[32]J. C. Snowdon, "Forced vibration of internally damped rectangular and square plates with simply supported boundaries," J. Acoust. Soc. Am. **56**, 1177–1184 (1974).
[33]J. C. Snowdon, "Vibration of simply supported rectangular and square plates to which lumped masses and dynamic vibration absorbers are attached," J. Acoust. Soc. Am. **57**, 646–654 (1975).
[34]E. Ventsel and T. Krauthammer, *Thin Plates and Shells* (Dekker, New York, 2004), pp. 1–14.
[35]G. Breit and E. Wigner, "Capture of slow neutrons," Phys. Rev. **49**, 519–531 (1936).
[36]P. M. Morse and K. U. Ingard, *Theoretical Acoustics* (Princeton University Press, Princeton, NJ, 1986), pp. 128–226.
[37]H. Statz and C. L. Tang, "Phase locking of modes in lasers," J. Appl. Phys. **36**, 3923–3927 (1965).
[38]C. L. Tang and H. Statz, "Maximum-emission principle and phase locking in multimode lasers," J. Appl. Phys. **38**, 2963–2968 (1967).
[39]M. Práger, "Eigenvalues and eigenfunctions of the Laplace operator on an equilateral triangle," Appl. Math. (Germany) **43**, 311–320 (1998).